A Modified Finite-Element Method for Dielectric Waveguides Using an Asymptotically Correct Approximation on Infinite Elements

Jan A. M. Svedin, *Student Member, IEEE*

Abstract—**A modified finite-element method for the propagation analysis of such dielectric waveguides as optical fibers and integrated optical waveguides is presented. Possible applications include nondissipative structures of arbitrary anisotropic media with, in some cases, inhomogeneous exterior regions. The method is based on the full vectorial finite-element formulation [7], which is known to be without spurious solutions. With this formulation all appropriate boundary and interelement conditions on both tangential and normal components are *a priori* satisfied. For the unbounded, exterior region a novel type of asymptotically correct approximation on infinite elements is proposed that simultaneously, for each mode and frequency, locally adapts the rate of radial decay to the transversal wavenumbers. The linearity of the original finite-element method has been retained by using β/k_0 as a parameter, which results in a sparse generalized eigenvalue problem. Numerical examples including both optical fibers and integrated optical waveguides, isotropic as well as anisotropic, have been analyzed to confirm the validity of the method. The observed correspondence with analytical solutions has been found to be excellent. For some examples a special near-field wavenumber has been added to preserve a high accuracy close to cutoff.**

I. Introduction

THE finite-element method (FEM) has during the last two decades become a well-established tool for propagation analysis of various waveguide components [1]–[8] for which closed-form analytical solutions cannot be found. In extending the FEM to handle open dielectric waveguide structures, which are becoming increasingly important for integrated optical devices and optical communication systems, a variety of approaches have been proposed.

With the artificial or virtual boundary technique both interior and exterior regions are treated using standard finite elements. The latter region is, however, truncated by, e.g., enclosing the entire waveguide structure within a perfect electric conductor [9] or requiring the fields to vanish at a certain distance from the origin [10]. A disadvantage is that the location of the artificial boundary yielding the most accurate solution is not known in advance. It can, however, be determined iteratively for each mode and frequency [11].

Hybrid methods combine the standard FEM with methods more compatible with open regions, such as function expansion [12] or integral equation methods [13], [14]. The hybrid methods are often restricted to waveguides with a homogeneous exterior region, such as optical fibers, and result in nonlinear systems of equations. The latter is due to the necessity of knowing the transversal wavenumber in order to evaluate the Hankel functions appearing in both the function expansion and integral equation methods. As the transversal wavenumber is unknown at the outset of the problem, the linearity is lost.

Modified FEM's combine the standard FEM with a special treatment of the exterior region, e.g. using an expansion on infinite elements. One example is [15], which utilizes a parametric infinite element with a radial trial function $\gamma = e^{-\alpha r}$, where $1/\alpha$ is a global decay length. As the decay length is initially unknown, an outer iteration loop has to be run through for each mode and frequency to determine the optimum value of α. As different coordinate systems are used for the interior and exterior regions, interelement conditions cannot be satisfied exactly along the interface between the standard and special elements. A similar approach, but formulated in terms of Cartesian coordinates, that allows an exact fulfillment of the boundary conditions is described in [16]. Iterative procedures are proposed in [17] that allow a self-consistent determination of the optimum decay length by using either the previous eigenvalue or eigenvector. A different approach is proposed in [18], one that removes the need to iterate for an optimum decay parameter. Instead, a set of decay lengths is selected to allow for adequate modelling of the asymptotic behavior of all modes of interest. The choice of decay lengths has to be made by the user. Only isotropic guides with homogeneous core and cladding are treated in [18].

In this paper a modified FEM is proposed which for the exterior region uses an asymptotically correct approximation on symmetrical infinite elements, through which the local rate of radial decay is adapted to the transversal wavenumbers simultaneously for all modes and frequencies. The need to iterate for an optimum decay parameter is thus avoided. The linearity of the original FEM has been retained by using the normalized propagation constant, β/k_0, as a parameter, which results in a sparse generalized eigenvalue problem for which very efficient solvers exist.

The method presented here is based on the full vectorial $(\boldsymbol{E}-\boldsymbol{H})$ finite-element formulation [7], [8], which is directly derived from the first-order Maxwell curl equations and which *a priori* enforces not only the necessary conditions on the tangential components $\boldsymbol{n}\times\boldsymbol{E}$ and $\boldsymbol{n}\times\boldsymbol{H}$, but also the additional conditions on the normal components $\boldsymbol{n}\cdot\boldsymbol{B}$ and

Manuscript received February 22, 1990; revised August 2, 1990.

The author is with the Department of Information Technology (FOA3), Swedish Defence Research Establishment, P.O. Box 1165, S-581 11 Linköping, Sweden.

IEEE Log Number 9041077.

0018-9480/91/0200-0258$01.00 ©1991 IEEE

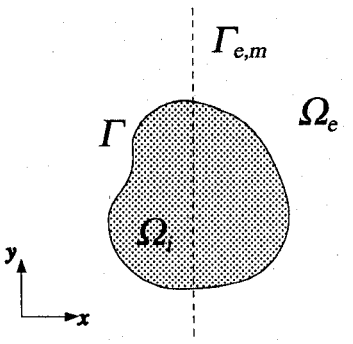

Fig. 1. The arbitrary, open dielectric waveguide structure.

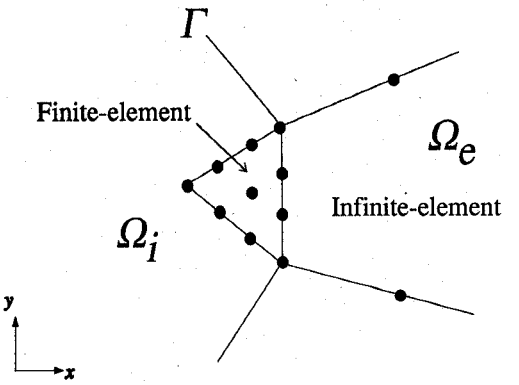

Fig. 2. A portion of a sample finite/infinite-element mesh employing third-order interpolation.

$\boldsymbol{n}\cdot\boldsymbol{D}$. With this formulation an absence of spurious modes has earlier been found.

A number of numerical examples covering both optical fibers and integrated optical waveguides, isotropic as well as anisotropic, have been analyzed in order to evaluate the validity of the presented method. For some examples a special near-field wavenumber has been added in order to preserve a high accuracy close to cutoff.

II. Mathematical Derivation

A. The Boundary-Value Problem

In this paper we consider open dielectric waveguide structures of the type depicted in Fig. 1, which consists of an interior region, Ω_i, containing the possibly inhomogeneous core, an exterior region, Ω_e, containing the possibly inhomogeneous cladding, an interface between the two regions, Γ, and possible electric and magnetic walls, Γ_e and Γ_m, respectively. The structure is assumed nondissipative but may otherwise consist of arbitrary linear media, each described by relative permittivity and permeability self-adjoint matrices $[\epsilon]$ and $[\mu]$, respectively. Assuming a harmonic time dependence of the form $e^{j\omega t}$, where ω is the real angular frequency, the governing source-free Maxwell equations are

$$\nabla\times\boldsymbol{E}=-j\omega\boldsymbol{B}=-j\omega\mu_0[\mu]\boldsymbol{H} \tag{1}$$

$$\nabla\times\boldsymbol{H}=j\omega\boldsymbol{D}=j\omega\epsilon_0[\epsilon]\boldsymbol{E} \tag{2}$$

where $\boldsymbol{E}$, $\boldsymbol{H}$, $\boldsymbol{D}$, $\boldsymbol{B}$, ϵ_0, and μ_0 are, respectively, the electric field, the magnetic field, the electric displacement, the magnetic induction, the permittivity of vacuum, and the permeability of vacuum. For the boundary-value problem to be well-defined, it is necessary to enforce the boundary and continuity conditions on the tangential field components $\boldsymbol{n}\times\boldsymbol{E}$ and $\boldsymbol{n}\times\boldsymbol{H}$.

B. The Weak Formulation

The presented method is based on the full vectorial [19] weak formulation [7] of the boundary-value problem as straightforwardly derived from the first-order curl equations (1) and (2). Approximate weak solutions [20] $\boldsymbol{E}$ and $\boldsymbol{H}$ are hereby forced to satisfy

$$\iint_{\Omega_i+\Omega_e}\left(\boldsymbol{E}^*_{\text{test}}\cdot\left(j\nabla\times\boldsymbol{H}+\omega\epsilon_0[\epsilon]\boldsymbol{E}\right)+\boldsymbol{H}^*_{\text{test}}\cdot\left(-j\nabla\times\boldsymbol{E}+\omega\mu_0[\mu]\boldsymbol{H}\right)\right)dS=0 \tag{3}$$

for admissible [20] test functions $\boldsymbol{E}_{\text{test}}$ and $\boldsymbol{H}_{\text{test}}$. The fields $\boldsymbol{E}$, $\boldsymbol{H}$, $\boldsymbol{E}_{\text{test}}$, and $\boldsymbol{H}_{\text{test}}$ should satisfy the appropriate interelement and boundary conditions. Here, we enforce interelement continuity of the tangential components, i.e.,

$$\boldsymbol{n}\times(\boldsymbol{E}_i-\boldsymbol{E}_j)=0 \tag{4}$$

$$\boldsymbol{n}\times(\boldsymbol{H}_i-\boldsymbol{H}_j)=0 \tag{5}$$

and of the normal components, i.e.,

$$\boldsymbol{n}\cdot(\boldsymbol{B}_i-\boldsymbol{B}_j)=\boldsymbol{n}\cdot\mu_0\left([\mu_i]\boldsymbol{H}_i-[\mu_j]\boldsymbol{H}_j\right)=0 \tag{6}$$

$$\boldsymbol{n}\cdot(\boldsymbol{D}_i-\boldsymbol{D}_j)=\boldsymbol{n}\cdot\epsilon_0\left([\epsilon_i]\boldsymbol{E}_i-[\epsilon_j]\boldsymbol{E}_j\right)=0 \tag{7}$$

where $\boldsymbol{n}$ is the unit vector at the interface between two adjacent elements i and j. We also enforce the tangential boundary conditions,

$$\boldsymbol{n}\times\boldsymbol{E}_i=0 \tag{8}$$

$$\boldsymbol{n}\times\boldsymbol{H}_i=0 \tag{9}$$

on Γ_e and Γ_m, respectively, and the corresponding normal conditions,

$$\boldsymbol{n}\cdot\boldsymbol{B}_i=\boldsymbol{n}\cdot\mu_0[\mu_i]\boldsymbol{H}_i=0 \tag{10}$$

$$\boldsymbol{n}\cdot\boldsymbol{D}_i=\boldsymbol{n}\cdot\epsilon_0[\epsilon_i]\boldsymbol{E}_i=0. \tag{11}$$

C. The Expansion in Ω_i

For the finite interior region, Ω_i, standard Nth-order triangular finite elements [20], [21] are employed, as illustrated in Fig. 2, which shows a portion of a sample finite/infinite-element mesh. The six components of the electric and magnetic fields are then approximated over each element in terms of the values at each of the finite-element nodal points according to

$$\begin{aligned}
E_x&=Z_0\{N\}^T\{E_x\}e^{-j\beta z}\\
E_y&=Z_0\{N\}^T\{E_y\}e^{-j\beta z}\\
E_z&=jZ_0\{N\}^T\{E_z\}e^{-j\beta z}\\
H_x&=\{N\}^T\{H_x\}e^{-j\beta z}\\
H_y&=\{N\}^T\{H_y\}e^{-j\beta z}\\
H_z&=j\{N\}^T\{H_z\}e^{-j\beta z}
\end{aligned} \tag{12}$$

where β is the propagation constant, and $Z_0=(\mu_0/\epsilon_0)^{1/2}$ is the intrinsic impedance of vacuum. The real $M\times 1$ column vector $\{N\}$ is the finite-element shape function vector, where $M=(N+1)(N+2)/2$ is the number of nodal points on each

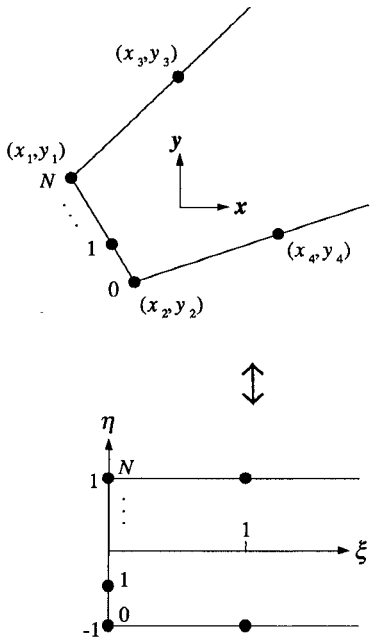

Fig. 3. The mapping of an infinite element from the $x-y$ to the $\eta-\xi$ plane.

element, and T denotes a matrix transposition. The construction of finite-element shape functions has been thoroughly described elsewhere [20], [21]. Here, the column vectors $\{E_x\}$, $\{E_y\}$, $\{E_z\}$, $\{H_x\}$, $\{H_y\}$, and $\{H_z\}$ are $M\times 1$ complex field vectors representing the nodal point values of, respectively, E_x/Z_0, E_y/Z_0, $-jE_z/Z_0$, H_x, H_y, and $-jH_z$ on each finite element.

D. The Expansion in Ω_e

For the infinite exterior region, Ω_e, a new type of expansion on symmetrical infinite elements [18] (see Fig. 3) is used, one that simultaneously for each mode and frequency adapts the local rate of radial decay to the transversal wavenumbers related to each medium. This approximation is asymptotically correct in the limit of infinite frequency or, correspondingly, in the limit of infinite radial distance. A brief derivation of this expansion follows.

To satisfy conditions (4)–(11) exactly along Γ, i.e., on all edges shared by finite and infinite elements, as exemplified in Fig. 2, standard Nth order Lagrange interpolation is used in the "azimuthal" direction, $-1\leqslant\eta\leqslant 1$, $\xi=$ constant (the mapping from the $\eta-\xi$ plane to the $x-y$ plane, $x=x(\eta,\xi)$, $y=y(\eta,\xi)$ is given in [18]). In this way the enforcement of continuity becomes trivial; the proper field components are simply equated at each nodal point along Γ. Any Cartesian field component, ψ, is hence expanded according to

$$\psi=\sum_{i=0}^{N}\Xi_i(\xi)H_i(\eta) \tag{13}$$

where the z dependence $e^{-j\beta z}$ has been omitted for brevity. In (13)

$$H_i(\eta)=\sum_{k=0}^{N}C_{i,k}\eta^k \tag{14}$$

is the Lagrange interpolation function associated with node i, defined by $H_i(\eta)=1$ at node i and $H_i(\eta)=0$ at nodes $j\neq i$, $j=0,\cdots,N$. The coefficients $C_{i,k}$ are tabulated in [18] for $N\leqslant 4$ but note that the node numbering differs. The factors $\Xi_i(\xi)$ are as yet unknown functions that determine the radial field behavior, which is to be governed locally (at each node) by the transversal wavenumbers. For strictly isotropic and homogeneous Ω_e, with transversal wavenumbers that are single valued and constant, respectively, a single exponential term suffices in the expression for $\Xi_i(\xi)$. For problems with anisotropic and/or inhomogeneous Ω_e, multiple wavenumbers are required in the expansion at some nodes (see below); therefore the following construction is employed:

$$\Xi_i(\xi)\equiv\sum_{j=1}^{m_i}a_{i,j}e^{-k_0\overline{W}_{i,j}(\overline{\beta})s_i\xi}. \tag{15}$$

Here $\overline{W}_{i,j}=W_{i,j}/k_0$ are normalized transversal wavenumbers to be defined below (with $W_{i,j}$ being the transversal wavenumbers), $a_{i,j}$ are unknown constants to be determined, $k_0=\omega/c_0=\omega(\epsilon_0\mu_0)^{1/2}$ is the vacuum wavenumber, m_i is the number of exponential terms used at each node, $\overline{\beta}=\beta/k_0$ is the normalized propagation constant, and

$$s_i=\left.\frac{\partial\left(\sqrt{x^2+y^2}\right)}{\partial\xi}\right|_{\eta=-1+2i/N}. \tag{16}$$

The factors s_i, which are independent of ξ, are necessary because the length elements $d\xi$ and $d(\sqrt{x^2+y^2})$ usually differ.

The determination of $\overline{W}_{i,j}$ will now be explained. Bearing in mind that (13) at each nodal point i consists of damped plane waves $e^{jk_0\bar{k}_{i,j}\cdot r}$, where

$$\begin{cases}\bar{k}_{i,j}=\dfrac{k_{i,j}}{k_0}=j\overline{W}_{i,j}(\overline{\beta})s_i\xi-\overline{\beta}z\\ r=\xi\xi+zz.\end{cases} \tag{17}$$

Consistency requires that an expression $e^{jk_0\bar{k}_i\cdot r}$ with

$$\bar{k}_i=j\overline{W}_i(\overline{\beta})s_i\xi-\overline{\beta}z$$

be used to calculate $\overline{W}_{i,j}$, by solving (1) and (2) for a given $\overline{\beta}$.

For an isotropic medium the transversal wavenumber is well known to be $W_{i,1}=(\beta^2-k_0^2n^2)^{1/2}$, where $n=(\epsilon_r\mu_r)^{1/2}$ is the refractive index, ϵ_r is the relative permittivity, and μ_r is the relative permeability. The single resulting normalized transversal wavenumber thus becomes $\overline{W}_{i,1}=(\overline{\beta}^2-n^2)^{1/2}$, from which $m_i=1$ in (15).

For an anisotropic medium with tensor permittivity $[\epsilon]$ and scalar permeability μ_r, which is the most usual anisotropic case, the resulting wavenumbers are found from Fresnel's equation [22],

$$\left|n^2\delta_{v,v'}-n_vn_{v'}-\mu_r\epsilon_{v,v'}\right|=0 \tag{18}$$

where

$$\boldsymbol{n}=\bar{\boldsymbol{k}}_i=j\overline{W}_i(\overline{\beta})s_i(\cos\varphi\boldsymbol{x}+\sin\varphi\boldsymbol{y})-\overline{\beta}\boldsymbol{z} \tag{19}$$

should not be confused with the $\boldsymbol{n}$ in (4)–(11); n is the generalized refractive index, $\delta_{v,v'}$ is the Kronecker delta, $v,v'=x$, y, z, and φ is the angle from $\boldsymbol{x}$ to $\boldsymbol{\xi}$. As it turns out, (18) becomes a polynomial equation in $\overline{W}_i$, whose solutions yield the possible wavenumbers $\overline{W}_{i,j}$, $j=1,\cdots,m_i\leqslant 2$ in (15).

As the present analysis is restricted to lossless structures above cutoff, all $\overline{W}_{i,j}$ have to be real. They also have to be positive to guarantee the radial decay, because only positive k_0 are accepted when solving the resulting eigenvalue problem, for which k_0 constitutes the eigenvalue (see (33) below).

If Ω_e is inhomogeneous, which is the case for integrated optical waveguides, individual wavenumbers have to be calculated for each medium. Some infinite-element nodes ($i = 0$ or N) will then reside on interfaces between two different media with separate wavenumbers. The enforcement of (4)–(11) that is required by the FEM along such an interface seems impossible. However, by including wavenumbers related to both the media in the expansion on both sides of the interface, this problem is avoided. A disadvantage is that m_t increases locally and the radial decay will not be asymptotically correct near the interface. The latter is, however, believed to be of negligible importance. A remedy is to insert narrow "transition" elements on each side of the interfaces in this category.

The infinite-element expansion as introduced thus far is likely to yield accurate results at least for modes that are sufficiently high above cutoff that the assumed exponential behavior gives a good approximation of the correct field behavior. A relevant quantity is $k_0\overline{W}a$, where a is a characteristic dimension of Ω_t. The approximation may deteriorate as $k_0\overline{W}a \to 0$ if the near-field behavior is not of the assumed exponential form. For such a situation two measures are suggested that will preserve the accuracy closer to cutoff: a) an increase of a by moving Γ further away from the core and b) the inclusion of one or more near-field wavenumbers [18], which should be larger in magnitude than the asymptotic wavenumbers discussed above, thus permitting more rapid variations to be modeled. In this work the second measure was used with one near-field wavenumber for some examples to maintain a high accuracy close to cutoff. This subject is further discussed in the numerical examples.

In keeping the notation in terms of shape function vectors, we obtain for each infinite element the following expansion:

$$\begin{aligned} E_x &= Z_0\{N_\infty\}^T\{E_x\}e^{-j\beta z} \\ E_y &= Z_0\{N_\infty\}^T\{E_y\}e^{-j\beta z} \\ E_z &= jZ_0\{N_\infty\}^T\{E_z\}e^{-j\beta z} \\ H_x &= \{N_\infty\}^T\{H_x\}e^{-j\beta z} \\ H_y &= \{N_\infty\}^T\{H_y\}e^{-j\beta z} \\ H_z &= j\{N_\infty\}^T\{H_z\}e^{-j\beta z} \end{aligned} \tag{20}$$

where the component of the infinite-element shape function vector, $\{N_\infty\}$, associated with wavenumber $\overline{W}_{t,j}$, $i = 0, \cdots, N$, $j = 1, \cdots, m_t$, is

$$H_t(\eta)e^{-k_0\overline{W}_{t,j}(\bar{\beta})s_t\xi}. \tag{21}$$

Here $\{E_x\}$, $\{E_y\}$, $\{E_z\}$, $\{H_x\}$, $\{H_y\}$, and $\{H_z\}$ have the same meanings as in (12) but with a different dimension, namely $m_0 + m_1 + \cdots + m_N$ on each infinite element.

E. The Generalized Eigenvalue Problem

By applying the standard Galerkin procedure to (3) with the finite-element expansion (12) and the infinite-element expansion (20), and treating $\bar{\beta}$ as a parameter, there results the following quadratic generalized eigenvalue problem:

$$\left([P_0] + \bar{\beta}[Q_0] + \frac{1}{k_0}([R_0] + [P_1] + \bar{\beta}[Q_1] + [R_1]) + \frac{1}{k_0^2}([P_2] + \bar{B}[Q_2] + [R_2])\right)\{\Phi\} = \{0\} \tag{22}$$

where $\{\Phi\}$ is a column vector composed of all the unknowns used to represent $\boldsymbol{E}$ and $\boldsymbol{H}$ throughout the entire waveguide cross section. Here, $1/k_0$ constitutes the eigenvalue. The matrices with index zero are finite-element matrices (cf. [7]), while the other matrices are infinite-element matrices. The square, sparse matrices $[P_i]$, $[Q_i]$, and $[R_i]$, $i = 0, 1, 2$, are

$$[P_t] = \sum_e \begin{bmatrix} \epsilon_{xx}[A_t] & \epsilon_{xy}[A_t] & j\epsilon_{xz}[A_t] & [0] & [0] & [0] \\ \epsilon_{yx}[A_t] & \epsilon_{yy}[A_t] & j\epsilon_{yz}[A_t] & [0] & [0] & [0] \\ -j\epsilon_{zx}[A_t] & -j\epsilon_{zy}[A_t] & \epsilon_{zz}[A_t] & [0] & [0] & [0] \\ [0] & [0] & [0] & \mu_{xx}[A_t] & \mu_{xy}[A_t] & j\mu_{xz}[A_t] \\ [0] & [0] & [0] & \mu_{yx}[A_t] & \mu_{yy}[A_t] & j\mu_{yz}[A_t] \\ [0] & [0] & [0] & -j\mu_{zx}[A_t] & -j\mu_{zy}[A_t] & \mu_{zz}[A_t] \end{bmatrix} \tag{23}$$

$$[Q_i] = \sum_e \begin{bmatrix} [0] & [0] & [0] & [0] & -[A_t] & [0] \\ [0] & [0] & [0] & [A_t] & [0] & [0] \\ [0] & [0] & [0] & [0] & [0] & [0] \\ [0] & [A_i] & [0] & [0] & [0] & [0] \\ -[A_t] & [0] & [0] & [0] & [0] & [0] \\ [0] & [0] & [0] & [0] & [0] & [0] \end{bmatrix} \tag{24}$$

$$[R_i] = \sum_e \begin{bmatrix} [0] & [0] & [0] & [0] & [0] & -[C_t] \\ [0] & [0] & [0] & [0] & [0] & [B_t] \\ [0] & [0] & [0] & -[C_t] & [B_t] & [0] \\ [0] & [0] & [C_i] & [0] & [0] & [0] \\ [0] & [0] & -[B_i] & [0] & [0] & [0] \\ [C_i] & -[B_i] & [0] & [0] & [0] & [0] \end{bmatrix} \tag{25}$$

where Σ_e denotes the matrix assembly procedure [21], in which rows and columns corresponding to test and expansion functions associated with variables in the unconnected system are connected according to the interelement and boundary conditions (4)–(11). In (23)–(25), the nonvanishing matrix elements are

$$[A_0] = \iint_e \{N\}\{N\}^T dS \tag{26}$$

$$[B_0] = \iint_e \{N\}\frac{\partial\{N\}^T}{\partial x} dS \tag{27}$$

$$[C_0] = \iint_e \{N\}\frac{\partial\{N\}^T}{\partial y} dS \tag{28}$$

$$\frac{[A_1]}{k_0} + \frac{[A_2]}{k_0^2} = \iint_e \{N_\infty\}\{N_\infty\}^T dS \tag{29}$$

$$[B_1] + \frac{[B_2]}{k_0} = \iint_e \{N_\infty\}\frac{\partial\{N_\infty\}^T}{\partial x} dS \tag{30}$$

$$[C_1] + \frac{[C_2]}{k_0} = \iint_e \{N_\infty\}\frac{\partial\{N_\infty\}^T}{\partial y} dS \tag{31}$$

where the integrations in (26)–(28) extend over a finite element and in (29)–(31) over an infinite element. Explicit expressions for the infinite-element matrices $[A_i]$, $[B_i]$, and $[C_i]$, $i = 1,2$, which depend only on the infinite-element geometry and the transversal wavenumbers, are given in the Appendix.

To linearize (22) as efficiently as possible we recognize that $\{\Phi\}$ can be divided into vectors $\{\Phi_{\in\Gamma}\}$ and $\{\Phi_{\notin\Gamma}\}$, of which the former contains only variables related to nodal points on Γ and the latter contains the remaining, strictly internal variables. As the infinite-element matrices operate only on $\{\Phi_{\in\Gamma}\}$, the following new variables are introduced:

$$\{\tilde{\Phi}_{\in\Gamma}\} = k_0^{-1}\{\Phi_{\in\Gamma}\} \tag{32}$$

which when used in (22) and after multiplication by k_0 yields

$$\begin{cases} (k_0([P_0]+\bar{\beta}[Q_0])+[R_0]+[P_1]+\bar{\beta}[Q_1]+[R_1])\{\Phi\} \\ \quad +([P_2]+\bar{\beta}[Q_2]+[R_2])\{\tilde{\Phi}_{\in\Gamma}\} = \{0\} \\ k_0\{\tilde{\Phi}_{\in\Gamma}\} - \{\Phi_{\in\Gamma}\} = \{0\} \end{cases} \tag{33}$$

which is the resulting linear generalized eigenvalue problem. The dimension of (33) equals the dimension of $\{\Phi_{\notin\Gamma}\}$ plus twice the dimension of $\{\Phi_{\in\Gamma}\}$. For large problems the former dimension is usually much larger than the latter. Correspondingly, most of the unknowns will be related to nodal points located strictly inside Ω_t.

By solving the sparse generalized eigenvalue problem (33) with $\bar{\beta}$ as the known parameter, all field components for the approximate fields of propagating eigenmodes are directly determined and the corresponding eigenvalues k_0 are found. From the knowledge of $\bar{\beta}$ and k_0, β is directly obtained. As $\bar{W}$ has been assumed real and positive, only real and positive values of k_0 are accepted, as discussed above.

III. Numerical Examples

With the aim of evaluating the validity of the presented method, a number of waveguide structures have been analyzed. Both optical waveguides and integrated optical waveguides, isotropic as well as anisotropic, have been considered. The solutions obtained have been compared with solutions reported elsewhere or, if available, analytical solutions. No spurious solutions [1]–[8] were observed during this work.

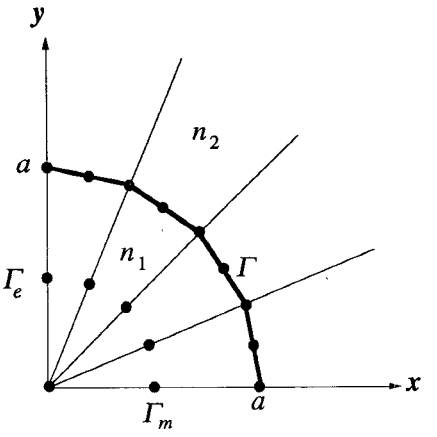

Fig. 4. The mesh used for the circular dielectric waveguide comprising four second-order triangles and four infinite elements.

The dense generalized eigenvalue NAG routine f02bjf [23] was used to calculate the eigenvalues and eigenvectors of (33). The computational load involved and the computer storage are proportional to R^3 and R^2, respectively, where R is the total number of unknowns. As pointed out before [7], [8], [16], [18], the use of a sparse [24] eigenvalue routine would significantly reduce the required amounts of computer time and memory, as the density of the matrices is of the $O(1/R)$ type; i.e., the maximum number of nonzero elements on each row is independent of R.

A. The Circular Dielectric Waveguide

The first example consists of a circular dielectric waveguide of radius a, core refractive index $n_1 = 1.53$, and cladding refractive index $n_2 = 1.50$ [15], [18]. The fundamental HE_{11} and higher order HE_{31} modes were calculated using the mesh shown in Fig. 4, which comprises four second-order triangles and four infinite elements (15 nodes). Only one quarter of the waveguide was meshed with electric and magnetic walls imposed on the two edges $x = 0$ and $y = 0$, respectively.

The resulting dispersion diagram is plotted in Fig. 5, where results of the presented method (squares) are compared with analytical solutions (solid lines) [25]. For the mesh used, a near-field wavenumber $\bar{W}_2 = M_{nf}\bar{W}_1$, where $\bar{W}_1$ is the asymptotic wavenumber discussed above, was included for values of $\bar{\beta}$ below 1.515. For this and the other example in this paper (subsection III-B) where a near-field term was used, M_{nf} was set to 5. The value of $\bar{\beta}$ where the asymptotic approximation starts to fail corresponds to $k_0\bar{W}_1 a \approx 1$. The result for the HE_{11} mode without the near-field term is plotted for comparison in Fig. 5 (circles). The addition of a near-field term did not influence the higher-order HE_{31} mode as much as the fundamental mode.

The dimension of (33) for this example was $26 + 2*48 = 122$ without the near-field term and $26 + 2*2*48 = 218$ with the near-field term. The dispersion diagram indicates a correspondence with the analytical solutions that is high, espe-

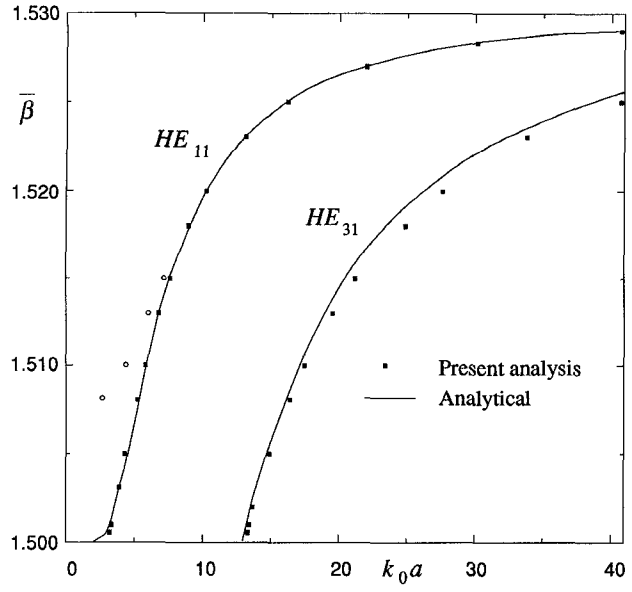

Fig. 5. The obtained propagation characteristics for the circular dielectric waveguide using the mesh illustrated in Fig. 4.

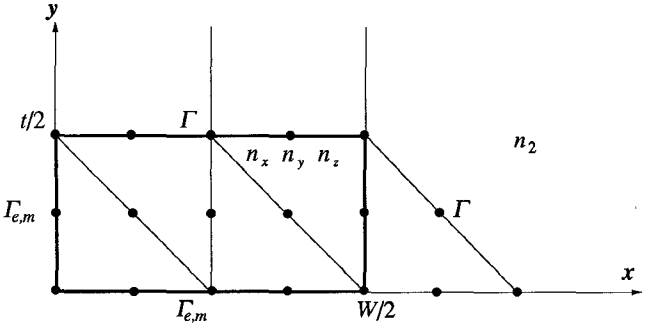

Fig. 6. The mesh used for the anisotropic dielectric rectangular waveguide comprising five second-order triangles and three infinite elements.

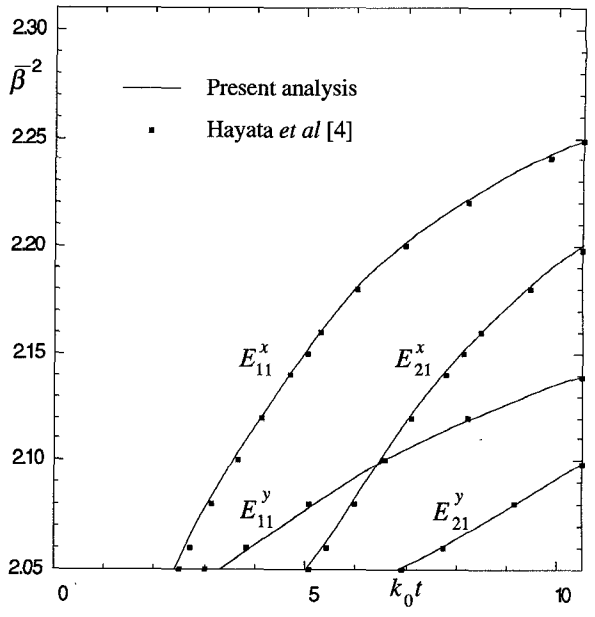

Fig. 7. The resulting dispersion diagram for the anisotropic dielectric rectangular waveguide using the mesh shown in Fig. 6.

cially for the fundamental mode, considering the relatively crude mesh. The maximum error in $\bar{\beta}$ was 0.07% for the HE_{11} mode and 0.08% for the HE_{31} mode.

To determine whether the asymptotic approximation is effective or not, one may of course always include one or more near-field terms. The calculated eigenvalues and eigenvectors will be weakly influenced by the incorporation of such terms if the field behavior actually is of the assumed exponential form.

B. The Anisotropic Rectangular Dielectric Waveguide

The second example consists of an anisotropic, rectangular, dielectric waveguide of height t, width $W = 2t$, core refractive indices $n_x^2 = n_y^2 = 2.31$, $n_z^2 = 2.19$, and cladding refractive index $n_2^2 = 2.05$ [4]. One quarter of the guide was meshed using five second-order triangles and three infinite elements (18 nodes), as illustrated in Fig. 6, to calculate the E_{11}^x, E_{11}^y, E_{21}^x, and E_{21}^y modes by assuming mode-dependent boundary conditions on the two edges $x = 0$ and $y = 0$ [26].

The resulting dispersion relations are plotted in Fig. 7, in which solid lines denote results using the present method and solid squares denote the FEM results of [4]. Also for this example a near-field wavenumber, $\bar{W}_2 = M_{\text{nf}}\bar{W}_1$, was added for values of $\bar{\beta}^2 \leqslant 2.10$ in order to obtain high accuracy throughout the whole dispersion diagram. Again, the value of $\bar{\beta}^2$ at which the asymptotic approximation starts to fail for the fundamental E_{11}^x mode corresponds to $k_0\bar{W}_1 a \approx 1$.

The dimension of (33) for the mesh shown in Fig. 6 was $44 + 2*39 = 122$ without the near-field term and $44 + 2*2*39 = 200$ with the near-field term. Hayata *et al.* [4] analyzed the waveguide considered using a finite-element formulation in terms of the magnetic field and with artificial boundary conditions for truncation of the exterior region. The present results show a high correspondence with their results as well as with the variational method [27].

C. The Anisotropic Slab Integrated Waveguide

This example consists of a one-dimensional, anisotropic, asymmetric slab waveguide. It is a $t = 50$ μm thick slab with refractive indices $n_x = 2.20001$, $n_y = 2.25002$, and $n_z = 2.30004$ on a substrate with indices $n_x' = 2.20000$, $n_y' = 2.25000$, and $n_z' = 2.30000$ and a surrounding refractive index $n_0 = 1$. A mesh comprising four fourth-order triangles and two infinite elements (41 nodes), as shown in Fig. 8, was used for comparison with exact solutions reported in [28]. For the fundamental TE_1 and TM_1 modes, perfect electric and magnetic walls, respectively, were assumed at the external edges at $x = 0$, $\Delta \to 0$. The number of unknowns was $168 + 2*48 = 264$ for the TM mode and $168 + 2*72 = 312$ for the TE mode; the solution of (18) in the substrate yields one solution for $\bar{\beta} < 2.25000$ but two solutions for $\bar{\beta} > 2.25000$.

Results for certain values of $\bar{\beta}$ are given in Table I where $\lambda = k_0^2(n_r^2 - \bar{\beta}^2)$. The correspondence with the analytical solutions is excellent considering the extremely small change in refractive indices between the slab and substrate and compares well with the finite-element results [28], where a zero-field condition was used at a large distance from the guide. The required computation time for 312 unknowns is of order 10^1 minutes for each value of $\bar{\beta}$ on a 1 Mflop computer,

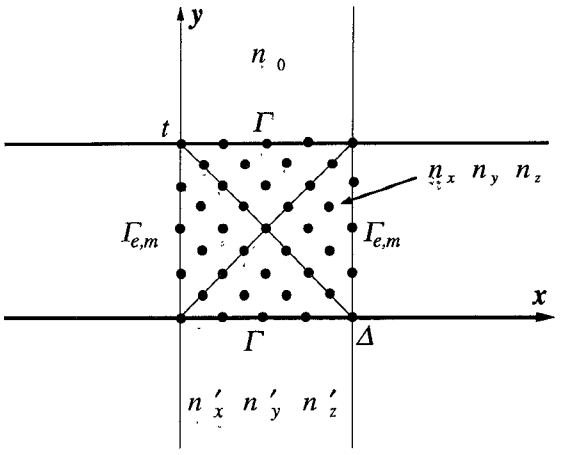

Fig. 8. The mesh used for the one-dimensional anisotropic slab waveguide comprising four fourth-order triangles and two infinite elements.

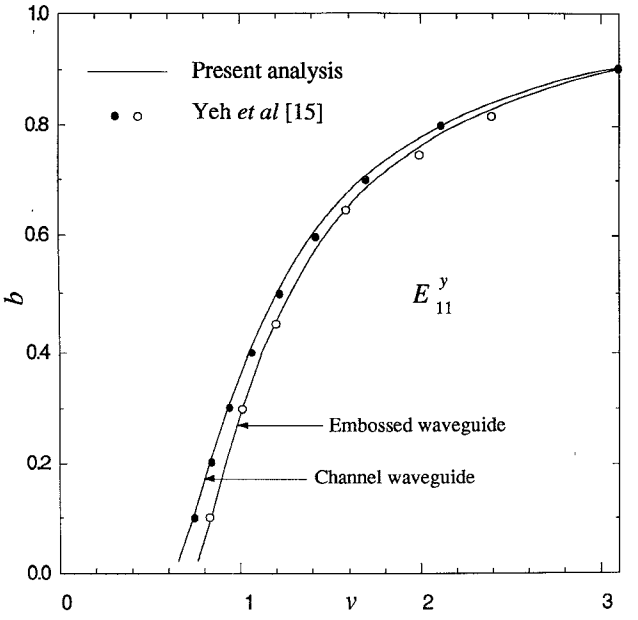

Fig. 10. The resulting propagation characteristics for the channel and embossed waveguides using the mesh illustrated in Fig. 9.

TABLE I
RESULTS FOR THE ANISOTROPIC ONE-DIMENSIONAL SLAB WAVEGUIDE

Mode	$\bar{\beta}$	λ (Exact)	λ	% Error
TE_1	2.200008	0.28653	0.28652	0.0034
$n_r = 2.20001$	2.200004	0.20302	0.20303	0.0035
TM_1	2.250016	0.27443	0.27447	0.0140
$n_t = 2.25002$	2.250008	0.19462	0.19462	0.0015

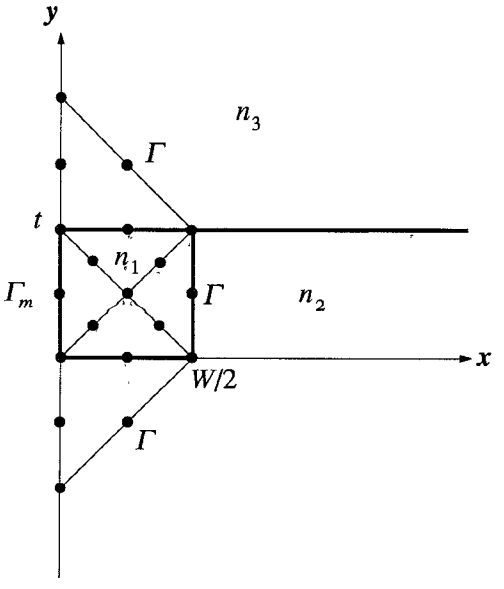

Fig. 9. The mesh used for the channel waveguide, the embossed waveguide, and the anisotropic channel waveguide, comprising six second-order triangles and three infinite elements.

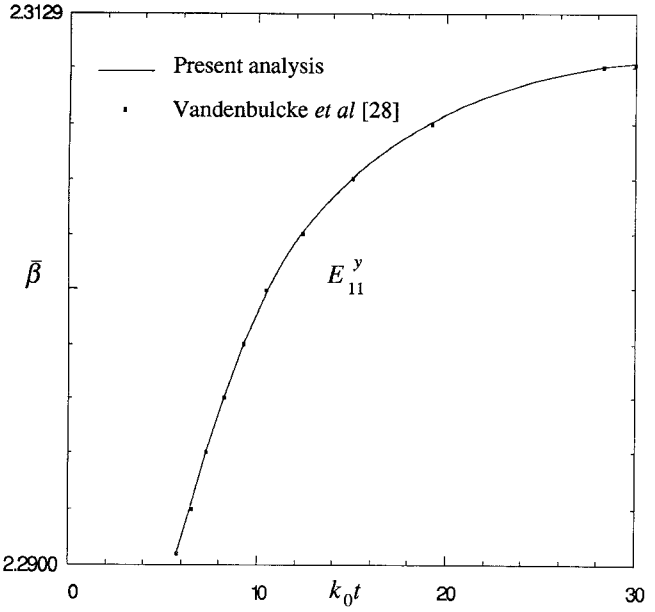

Fig. 11. The resulting dispersion relation for the fundamental mode of the anisotropic channel waveguide using the mesh shown in Fig. 9.

using the dense NAG routine. No near-field terms were necessary for this example.

D. The Embedded and Embossed Integrated Waveguides

The next two examples consist of a rectangular channel (embedded) waveguide and a rectangular embossed waveguide [15], [26]. Both waveguides are specified by the width $W = 2t$, the thickness t, and the refractive indices n_1, n_2, and n_3. The channel waveguide has $n_1 = 1.50$, $n_2 = 1.45$, and

$n_3 = 1.00$, while the embossed waveguide has $n_1 = 1.50$, $n_2 = 1.00$, and $n_3 = 1.45$. The mesh shown in Fig. 9, which comprises six second-order triangles and three infinite elements (19 nodes), was used for both guides to calculate the fundamental E_{11}^y mode by imposing a magnetic wall at the edge $x = 0$. No near-field terms were used for this example.

The resulting dispersion relations are shown in Fig. 10, where the present results (solid lines) are compared with the finite-element results [15] (dots and circles). Here, $b = (\bar{\beta}^2 - n_s^2)/(n_c^2 - n_s^2)$, where n_s and n_c are the refractive indices of the substrate and the core, respectively, and $v = tk_0(n_c^2 - n_s^2)^{1/2}/\pi$. The correspondence with the finite-element results of [15] is very high. The dimension of (33) for these problems was $63 + 2*50 = 163$.

E. The Anisotropic Channel Integrated Waveguide

The last example [26], [28] consists of an $LiNbO_3$ anisotropic channel waveguide of width $W = 5t$, thickness t, core refractive indices $n_{1x} = 2.222$ and $n_{1y} = n_{1z} = 2.3129$, substrate refractive indices $n_{2x} = 2.20$ and $n_{2y} = n_{2z} = 2.29$, and surrounding refractive index $n_3 = 1$. The same mesh used for the isotropic channel and embossed waveguides shown in Fig. 9 was used for this waveguide to calculate the dispersion relation for the fundamental E_{11}^y mode by imposing a magnetic wall at $x = 0$. No near-field terms were used for this example.

The resulting diagram is plotted in Fig. 11, where the solid line denotes results of the present analysis and the squares denote the FEM results reported in [28]. The correspondence between the two methods is very high. The size of (33) for this example was $63 + 2*81 = 225$.

IV. Conclusions

A modified finite-element method for the propagation analysis of dielectric waveguide structures has been proposed. An asymptotically correct expansion on infinite elements in the exterior region that simultaneously for each mode and frequency adapts the local rate of radial decay to the transversal wavenumbers has been presented. Suggested applications include both isotropic and anisotropic dielectric waveguide structures with possibly inhomogeneous exterior regions. The method is based on the full vectorial finite-element formulation, which enforces both the necessary tangential conditions and the additional normal conditions. The absence of spurious modes has hereby been conserved. By using β/k_0 as a parameter for the generalized eigenvalue problem, the linearity of the original FEM has been preserved. A number of numerical examples, including both optical fibers and integrated optical waveguides, have been analyzed and the correspondence with analytical results and results reported elsewhere has been found to be excellent. For some examples (optical fibers) a near-field wavenumber was added in order to obtain a high accuracy close to cutoff.

Appendix

The matrix elements in the infinite-element matrices in (29)–(31) corresponding to a pair of unknowns associated with wavenumbers $\overline{W}_{i,j}$ and $\overline{W}_{i',j'}$ are given by

$$[A_1]_{i,i',j,j'} = \sum_{k,k'=0}^{N} C_{i,k}C_{i',k'}\left[\frac{1-(-1)^{k+k'+1}}{k+k'+1}\right] \cdot \left[\frac{J_1}{\overline{W}_{i,j}s_i + \overline{W}_{i',j'}s_{i'}}\right] \tag{A1}$$

$$[A_2]_{i,i',j,j'} = \sum_{k,k'=0}^{N} C_{i,k}C_{i',k'}\left[\frac{1-(-1)^{k+k'+1}}{k+k'+1}\right] \cdot \left[\frac{J_2}{\left(\overline{W}_{i,j}s_i + \overline{W}_{i',j'}s_{i'}\right)^2}\right] \tag{A2}$$

$$[B_1]_{i,i',j,j'} = \sum_{k,k'=0}^{N} C_{i,k}C_{i',k'}\left[\frac{1-(-1)^{k+k'+1}}{k+k'+1}\right] \cdot \left[\frac{-a_{0x}\overline{W}_{i',j'}s_{i'}}{\overline{W}_{i,j}s_i + \overline{W}_{i',j'}s_{i'}}\right] \tag{A3}$$

$$[B_2]_{i,i',j,j'} = \sum_{k,k'=0}^{N} C_{i,k}C_{i',k'}\left[\frac{1-(-1)^{k+k'+1}}{k+k'+1}\right] \cdot \left[\frac{-a_{1x}\overline{W}_{i',j'}s_{i'}}{\left(\overline{W}_{i,j}s_i + \overline{W}_{i',j'}s_{i'}\right)^2} + \frac{b_{1x}k'}{\overline{W}_{i,j}s_i + \overline{W}_{i',j'}s_{i'}}\right] + \sum_{k=0,k'=1}^{N} C_{i,k}C_{i',k'}\left[\frac{1-(-1)^{k+k'}}{k+k'}\right] \cdot \left[\frac{b_{0x}k'}{\overline{W}_{i,j}s_i + \overline{W}_{i',j'}s_{i'}}\right] \tag{A4}$$

$$[C_1]_{i,i',j,j'} = \sum_{k,k'=0}^{N} C_{i,k}C_{i',k'}\left[\frac{1-(-1)^{k+k'+1}}{k+k'+1}\right] \cdot \left[\frac{-a_{0y}\overline{W}_{i',j'}s_{i'}}{\overline{W}_{i,j}s_i + \overline{W}_{i',j'}s_{i'}}\right] \tag{A5}$$

$$[C_2]_{i,i',j,j'} = \sum_{k,k'=0}^{N} C_{i,k}C_{i',k'}\left[\frac{1-(-1)^{k+k'+1}}{k+k'+1}\right] \cdot \left[\frac{-a_{1y}\overline{W}_{i',j'}s_{i'}}{\left(\overline{W}_{i,j}s_i + \overline{W}_{i',j'}s_{i'}\right)^2} + \frac{b_{1y}k'}{\overline{W}_{i,j}s_i + \overline{W}_{i',j'}s_{i'}}\right] + \sum_{k=0,k'=1}^{N} C_{i,k}C_{i',k'}\left[\frac{1-(-1)^{k+k'}}{k+k'}\right] \cdot \left[\frac{b_{0y}k'}{\overline{W}_{i,j}s_i + \overline{W}_{i',j'}s_{i'}}\right] \tag{A6}$$

where the coefficients J_1 J_2, a_{0x}, a_{1x}, a_{0y}, a_{1y}, b_{0x}, b_{1x}, b_{0y}, and b_{1y} depend only on the infinite-element coordinates x_1, x_2, x_3, x_4, y_1, y_2, y_3, and y_4 shown in Fig. 3 according to the expressions given in [18]. For (A3)–(A6) to hold, the infinite elements must be symmetrical with respect to $\eta = 0$.

ACKNOWLEDGMENT

The author would like to thank Dr. L. E. Pettersson and Dr. L. O. Pettersson at the Swedish Defence Research Establishment for very helpful discussions.

REFERENCES

[1] Z. J. Csendes and P. Silvester, "Numerical solution of dielectric loaded waveguides: I—Finite-element analysis," *IEEE Trans. Microwave Theory Tech.*, vol. MTT-18, pp. 1124–1131, Dec. 1970.

[2] A. Konrad, "Vector variational formulation of electromagnetic fields in anisotropic media," *IEEE Trans. Microwave Theory Tech.*, vol. MTT-24, pp. 553–559, Sept. 1976.

[3] M. Hano, "Finite-element analysis of dielectric-loaded waveguides," *IEEE Trans. Microwave Theory Tech.*, vol. MTT-32, pp. 1275–1279, Oct. 1984.

[4] K. Hayata, M. Koshiba, M. Eguchi, and M. Suzuki, "Vectorial finite-element method without any spurious solutions for dielectric waveguiding problems using transverse magnetic-field component," *IEEE Trans. Microwave Theory Tech.*, vol. MTT-34, pp. 1120–1124, Nov. 1986.

[5] T. Angkaew, M. Matsuhara, and N. Kumagai, "Finite-element analysis of waveguide modes: A novel approach that eliminates spurious modes," *IEEE Trans. Microwave Theory Tech.*, vol. MTT-35, pp. 117–123, Feb. 1987.

[6] K. Hayata, K. Miura, and M. Koshiba, "Finite-element formulation for lossy waveguides," *IEEE Trans. Microwave Theory Tech.*, vol. 36, pp. 268–275, Feb. 1988.

[7] J. A. M. Svedin, "A numerically efficient finite-element formulation for the general waveguide problem without spurious modes," *IEEE Trans. Microwave Theory Tech.*, vol. 37, pp. 1708–1715, Nov. 1989.

[8] J. A. M. Svedin, "Propagation analysis of chirowaveguides using the finite-element method," *IEEE Trans. Microwave Theory Tech.*, vol. 38, pp. 1488–1496, Oct. 1990.

[9] C. Yeh, S. B. Dong, and W. Oliver, "Arbitrarily shaped inhomogeneous optical fiber or integrated opt. waveguides," *J. Appl. Phys.*, vol. 46, no. 5, May 1975.

[10] N. Mabaya, P. E. Lagasse, and P. Vandenbulcke, "Finite-element analysis of optical waveguides," *IEEE Trans. Microwave Theory Tech.*, vol. MTT-29, pp. 600–605, Jun. 1981.

[11] M. Ikeuchi, H. Sawami, and H. Niki, "Analysis of open-type dielectric waveguides by the finite-element iterative method," *IEEE Trans. Microwave Theory Tech.*, vol. MTT-29, pp. 234–239, Mar. 1981.

[12] K. Oyamada and T. Okoshi, "Two-dimensional finite-element method of propagation characteristics of axially nonsymmetrical optical fibers," *Radio Sci.*, vol. 17, no. 1, pp. 109–116, Jan.–Feb. 1982.

[13] C. C. Su, "A combined method for dielectric waveguides using the finite-element technique and the surface integral equations method," *IEEE Trans. Microwave Theory Tech.*, vol. MTT-34, pp. 1440–1446, Nov. 1986.

[14] C. G. Williams and G. K. Cambrell, "Numerical solution of surface waveguide modes using transverse field components," *IEEE Trans. Microwave Theory Tech.*, vol. MTT-22, pp. 329–330, Mar. 1974.

[15] C. Yeh, K. Ha, S. B. Dong, and W. P. Brown, "Single-mode optical waveguides," *Appl. Opt.*, vol. 18, no. 10, pp. 1490–1504, May 1979.

[16] B. M. A. Rahman and J. B. Davies, "Penalty function improvement of waveguide solution by finite elements," *IEEE Trans. Microwave Theory Tech.*, vol. MTT-32, pp. 922–928, Aug. 1984.

[17] K. Hayata, M. Eguchi, and M. Koshiba, "Self-consistent finite/infinite element scheme for unbounded guided wave problem," *IEEE Trans. Microwave Theory Tech.*, vol. 36, pp. 614–616, Sept. 1988.

[18] M. J. McDougall and J. P. Webb, "Infinite elements for the analysis of open dielectric waveguides," *IEEE Trans. Microwave Theory Tech.*, vol. 37, pp. 1724–1731, Nov. 1989.

[19] W. J. English, "Vector variational solutions of inhomogeneously loaded cylindrical waveguide structures," *IEEE Trans. Microwave Theory Tech.*, vol. MTT-19, pp. 9–18, Jan. 1971.

[20] R. Wait and A. R. Mitchell, *Finite Element Analysis and Applications*. Chichester: Wiley, 1985.

[21] P. P. Silvester and R. L. Ferrari, *Finite Elements for Electrical Engineers*. Cambridge: Cambridge University Press, 1983.

[22] L. D. Landau and E. M. Lifshitz, *Electrodynamics of Continuous Media*. Oxford: Pergamon Press, 1960.

[23] NAG Fortran library, Numerical Algorithms Group Ltd., Oxford, England.

[24] I. S. Duff, "Survey of sparse matrix research," *Proc. IEEE*, vol. 65, pp. 500–535, Apr. 1977.

[25] J. D. Jackson, *Classical Electrodynamics*. New York: Wiley, 1975.

[26] M. Koshiba, K. Hayata, and M. Suzuki, "Improved finite-element formulation in terms of the magnetic field vector for dielectric waveguides," *IEEE Trans. Microwave Theory Tech.*, vol. MTT-33, pp. 227–233, Mar. 1985.

[27] M. Ohtaka, "Analysis of the guided modes of the anisotropic dielectric rectangular waveguides" (in Japanese), *Trans. Inst. Electron. Commun. Eng. Japan*, vol. J64-C, pp. 674–681, Oct. 1981.

[28] P. Vandenbulcke and P. E. Lagasse, "Eigenmode analysis of anisotropic optical fibers or integrated optical waveguides," *Electron. Lett.*, vol. 12, pp. 120–122, Mar. 1977.

✠

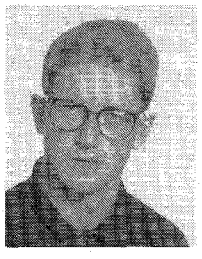

Jan A. M. Svedin (S'88) was born in Skellefteå, Sweden, on November 4, 1962. He received the M.Sc. degree in applied physics and electrical engineering in 1986 from the Linköping Institute of Technology, Linköping, Sweden.

Since 1987, he has been working as a research officer in the Division of Microwave Technology, Department of Information Technology, Swedish Defence Research Establishment, on the field analysis and design of dielectric resonator oscillators, microstrip antenna arrays, and ferrite control components. In addition, he is currently working toward the Ph.D. degree in theoretical physics at the Linköping Institute of Technology.